Phononic nodal points with quadratic dispersion and multifold degeneracy in the cubic compound Ta_3Sn

Tie Yang,[1,*] Chengwu Xie,[1,*] Hong Chen,[1] Xiaotian Wang,[1,†] and Gang Zhang[2,‡]
[1]*School of Physical Science and Technology, Southwest University, Chongqing 400715, China*
[2]*Institute of High Performance Computing, Agency for Science, Technology and Research, Singapore 138632, Singapore*

(Received 28 September 2021; accepted 10 March 2022; published 25 March 2022)

Topological states with quadratic dispersion and multiple-fold band degeneracy have not only fundamentally updated our knowledge of the phases of matter but also become a major cutting-edge research direction in condensed matter physics. Note that the sixfold band degeneracy corresponds to the maximum degeneracy in phononic systems. Remarkably, in this work, based on first-principles calculations, we proposed an authentic material, Ta_3Sn, which hosts phononic nodal points with both quadratic dispersion and maximum band degeneracy, i.e., quadratic contact triple point, quadratic contact Dirac point and sixfold-degenerate point. Furthermore, the corresponding symmetry analysis with the help of the $k \cdot p$ model further deepens the understanding of the relative physics. Evident arc-shaped surface states, originating from the projected phononic nodal points, can strongly benefit the experimental detection. It is hoped that the rich types of phonon points with quadratic dispersion and multiple-fold band degeneracy as well as the surface states can be confirmed in experiments soon.

DOI: 10.1103/PhysRevB.105.094310

I. INTRODUCTION

During the last decades, topological states in matter have sparked tremendous research interest, especially in the field of condensed matter physics [1–8]. Different from the elementary particles constrained by the Poincaré symmetry in high-energy physics, the topological emergent particles only need to comply with the crystal space-group symmetry. According to the Kramers degeneracy theorem, the lowest twofold band degeneracy is enforced within a time-reversal symmetric system, and if additional nonsymmorphic symmetries are introduced, other multiple-fold band degeneracies can be imposed at the Brillouin zone boundary, including triple, Dirac, sixfold, and eightfold band degeneracies [9–22]. These different topological states have been previously studied in electronic systems, both from experimental and theoretical perspectives [23–38].

Aside from the electrons, phonons are also present in condensed matter systems, and they correspond to the basic emergent bosons of the crystalline lattice [39,40]. Similar to electronic fermions, phononic bosons also share topological features from the lattice symmetry constrains, and several recent studies of topological states have expanded to this phononic boson systems [41–43]. Unlike topological states in electronic systems, where only the states in the vicinity of the Fermi energy level are interested, the topological phononic signatures can be examined in a very wide frequency region, because the phononic bosons are not restrained by the Pauli exclusion principle. Thus, larger degrees of freedom and higher potential of possibility are expected in topological phononic systems. Considerable progress has been made, recently, for example, topological Weyl phononic states were proposed in transition metal sulfides and silicides [44,45], Li_3CuS_2, BiIrSe, and MSi (M = Fe, Co, Mn, Re, Ru), and specifically, the double Weyl phonons have been experimentally verified in FeSi material [46]. Triple phononic nodal points are observed in ternary antimonide $Zr_3Ni_3Sb_4$ [47] and niobium phosphide materials NbX (X = P, As, Sb, Bi) [48], and a three-dimensional Dirac phonon is identified in a crystalline system with inversion symmetry [42].

More recently, in contrast to the conventional linear type, topological states with higher-order dispersion, like quadratic or cubic order, are brought into view by Wu and Yu *et al.* [49–51] in electronic systems, and they have aroused great research focus because more exotic properties can be produced. However, in the electronic system, the spin-orbital coupling effect often destroys or shifts the original topological states, leaving a strong obstacle to further development. With the arrival of the phononic system, a light is shed on the study of topological states with multiple-fold band degeneracy and higher-order band dispersion, which are rarely accessed in electronic systems but can be ideally examined within the phononic platform. At the moment, current studies of the phononic topological properties are still mainly focused on the topological state with low band degeneracy and linear band dispersion. For the topological phonon with higher-order band dispersions and multiple-fold band degeneracies, the relative research is extremely scarce. Different from the electronic fermions, eightfold topological point states cannot exist in such phononic systems due to the absence of a spin-orbital

*These authors contributed equally to this work.
†xiaotianwang@swu.edu.cn
‡zhangg@ihpc.a-star.edu.sg

coupling effect. Thus, the sixfold band degeneracy corresponds to the maximum degeneracy in phononic systems. Besides, the cubic order dispersion in phononic systems can only be present in the charge-4 Weyl point along a specific direction within a few space groups, leaving the quadratic order as the major higher-order dispersion [52,53]. In this sense, a fundamental question rises: *Is it possible to have topological states with both multiple-fold degeneracy and quadratic dispersion in a single phononic system?* If so, this could be very beneficial to serve as an ideal and universal material candidate to assess the corresponding topological properties.

In this work, based on first-principles calculations, we proposed a realistic material Ta_3Sn with cubic crystal structure, which can host phononic nodal points of both quadratic order and multiple degeneracy, i.e., quadratic contact triple point (QCTP), quadratic contact Dirac point (QCDP), and sixfold-degenerate point (SDP). Detailed band analysis and effective Hamiltonian models have been provided. The corresponding topological surface states are also verified, and clear arc-shaped phononic surface states originating from these projected nodal points are all observed, which can be very beneficial for future experimental observation. Our findings can thus significantly contribute to the study of topological phononic states with higher order, multiple degeneracy, or both.

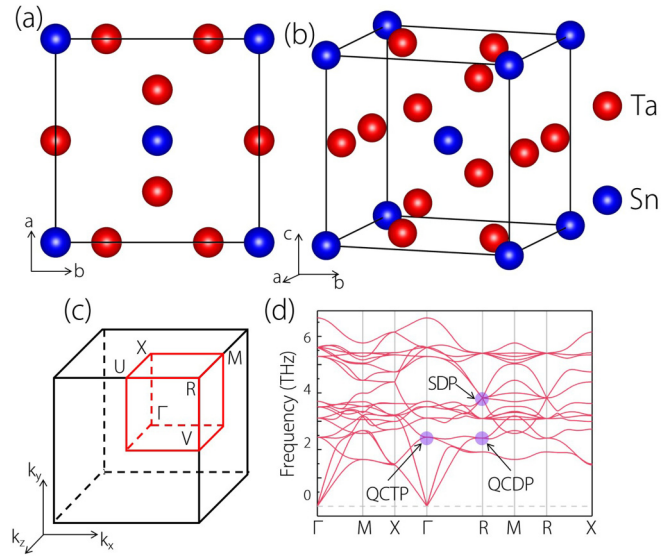

FIG. 1. The crystal structure of the cubic compound Ta_3Sn in different views (a) and (b). The corresponding Brillouin zone (c) with high-symmetry points and paths labeled. The calculated phonon dispersion curve (d) with the quadratic contact triple point (QCTP) at Γ point, quadratic contact Dirac point (QCDP), and sixfold-degenerate point (SDP) at R point indicated.

II. COMPUTATIONAL METHODOLOGY

First-principles calculations based on density functional theory [54] have been employed to study the ground state of the Ta_3Sn compound as implemented in the Vienna Ab initio Simulation Package VASP [55]. The projector augmented wave (PAW) method and the generalized gradient approximation (GGA) with Perdew-Burke-Ernzerhof (PBE) functional are used for the ionic potential and exchange-correlation interaction [56–58]. A plane-wave cutoff energy of 500 eV with $10\times10\times10$ k-mesh sampling was adopted for the structural relaxation and self-consistent field iteration, which are converged until the residual force variation per atom is less than 0.001 eV/Å and the total energy deviation is smaller than 1×10^{-6} eV. The Ta_3Sn compound has been experimentally synthesized with an arc furnace reaction, and it crystallizes in a cubic structure with space group $Pm\bar{3}n$ [59]. The fully optimized crystal lattice constants $a = b = c = 5.324$ Å are highly consistent with the experimental values $a = b = c = 5.276$ Å , and thus this relaxed structure is used for the following investigations. The phononic dispersion is examined by the density functional perturbation theory with the PHONOPY codes [60], and the topological surface properties are constructed by the WANNIERTOOLS package [61] based on the phononic Wannier tight-binding Hamiltonian.

III. RESULTS AND DISCUSSION

The crystal structure of Ta_3Sn compound is shown in Figs. 1(a) and 1(b) from different view angles, and its unit cell contains eight atoms, of which the two Sn atoms are located at the 2*a* Wyckoff sites (0, 0, 0) and the six Ta atoms are at the 6*c* Wyckoff sites (0.25, 0, 0.5). The corresponding first Brillouin zone of Ta_3Sn is shown in Fig. 1(c) with the selected high-symmetry points and paths marked. The phonon dispersion spectrum is calculated and shown in Fig. 1(d), from which two aspects can be directly observed: the acoustic branches are mixed with optical ones at low frequency, and the absence of an imaginary phonon mode indicates the dynamic stability of the Ta_3Sn compound. In the phononic dispersion, three areas with different situations of crossing points are focused in the current study, as highlighted with purple colors, namely, a QCTP at the Γ point, a QCDP, and an SDP at the R point. It should be mentioned here that the phononic system does not follow the restriction of the Pauli exclusion principle, and therefore, its topological signature can be ideally observed along the entire frequency range. We selected these three points as an example because they are well separated from other phonon bands, which is beneficial for the examination of their corresponding topological features. In the following discussion we investigate them and examine their topological properties individually.

First, we study the triply degenerate point at the Γ point in the 2.40–2.50 THz frequency range. It is located along the X-Γ-R path, and its band dispersion exhibits much larger variation at the X-Γ part than at the other Γ-R part. To have a better understanding for its formation, we have performed a full band scan in the $k_x = 0$ plane, and the results are shown in Fig. 2(a). Note that only the same three bands are selected, and we can see that all three bands contact together at the middle point, which corresponds to the triple point at the Γ position. Except for the triple point, the top band of purple color is well separated from the bottom two bands of green and red colors; the bottom two bands have also contacted along two lines, as shown by the yellow color lines, which are perpendicularly crossed at the Γ position. The quadratic dispersion order can be clearly observed from the band dispersions

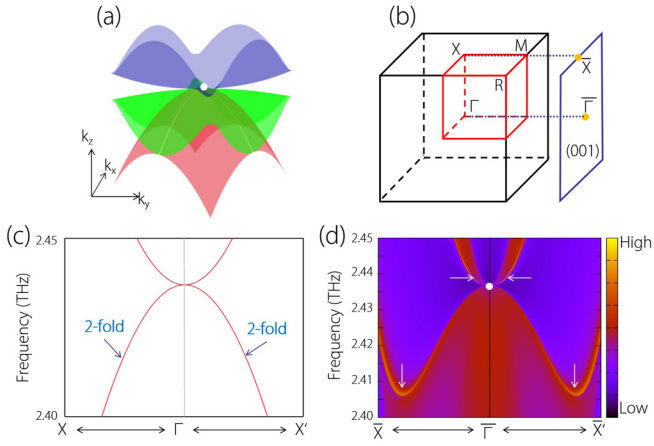

FIG. 2. The calculated phonon dispersion (a) around the QCTP, which is highlighted by the white dot. The (001) surface projection (b) of the bulk Brillouin zone. The local enlargement of the phonon band dispersion around the QCTP (c) and the corresponding (001) surface states projection, with the two arc-shaped spectra indicated by the white arrow.

along the X-Γ-X' path in the $k_x = 0$ plane, and the local enlargement is shown in Fig. 2(c). Such a triply degenerate point has been previously proposed in electronic band systems due to its special properties, and it is very rare compared with other common Weyl or Dirac fermions. In phononic band systems, this triply degenerate point exhibits a strong benefit, since the spin-orbital coupling effect, which often introduces a small gap for the triply degenerate point in the electronic system and thus shifts it to other topological phases, can be negligible. Such a triply degenerate point with quadratic order is even less explored and, due to the glide mirror symmetry, an effective Hamiltonian model has been constructed, as in Eq. (1), in which A_1, A_2, and B are real numbers. From the Hamiltonian, the total topological charge for this QCTP is derived and it is equal to zero, as typical for this spinless phononic system. The corresponding phonon surface state is also calculated in the (001) projected plane, see Fig. 2(b), and it is displayed in Fig. 2(d). The white dot represents the QCTP, and the arc-shaped surface states originating from the QCTP can be clearly seen, as indicated by the white arrows. Different from the triply degenerate point with linear dispersion, two arcs are found for this quadratic order:

$$H_{\mathrm{QCTP}}(\mathbf{k}) = \begin{bmatrix} A_1 k_x^2 + A_2\left(k_y^2 + k_z^2\right) & Bk_xk_y & Bk_xk_z \\ Bk_xk_y & A_1 k_y^2 + A_2\left(k_x^2 + k_z^2\right) & Bk_yk_z \\ Bk_xk_z & Bk_yk_z & A_1 k_z^2 + A_2\left(k_y^2 + k_x^2\right) \end{bmatrix}. \quad (1)$$

Next we discuss the Dirac point at the R position. It is located along the Γ-R-M path in the same frequency range of 2.40–2.50 THz. Similarly, a precise band scan has been calculated in the $k_y = \pi$ plane with the R point as the center, and the results are reported in Fig. 3(a), with only four bands selected. It is seen that the four bands exactly overlap at the plane center, forming a Dirac point as marked by the white dot. The quadratic order is clearly present from the band-surface dispersion around the central Dirac point, except that the top two bands with higher dispersion rate are separated from the bottom two ones of low dispersion rate. Besides, both the top and bottom two bands have constituted two perpendicular nodal lines. The surface states are also calculated on the $(\bar{1}10)$ plane, see Fig. 3(b), and the obtained local phononic densities of states are shown in Fig. 3(d). As a reference, the same phononic band dispersion near the Dirac point is shown in Fig. 3(c). Two arc surface states are emitted from the Dirac point, as indicated by the white arrows in the figure, and this is also introduced from the quadratic order band dispersion, the same as the above-discussed QCTP. Among the two arc states, the outside one is far separated from the bulk band, which is very beneficial for experimental observation. The corresponding effective Hamiltonian is also derived as in Eq. (2), in which $G^k = 2k_x^2 - k_y^2 - k_z^2$, $M^k = k_y^2 - k_z^2$, c_is are real parameters. Similar to QCTP, the total topological charge

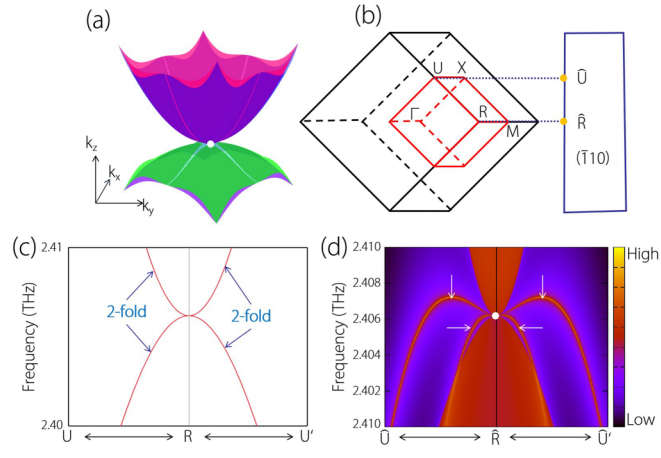

FIG. 3. The calculated phonon dispersion (a) around the QCDP, which is highlighted by the white dot. The $(\bar{1}10)$ surface projection (b) of the bulk Brillouin zone. The local enlargement of the phonon band dispersion around the QCDP (c) and the corresponding $(\bar{1}10)$ surface states projection, with the two arc-shaped spectra indicated by the white arrow.

for QCDP is equal to zero:

$$H_{\mathrm{QCDP}}(\mathbf{k}) = \begin{bmatrix} 0 & 0 & G^k(c_3 - ic_4) + \sqrt{3}M^k(-ic_3 - c_4) & 0 \\ 0 & 0 & 0 & G^k(c_3 - ic_4) + \sqrt{3}M^k(ic_3 + c_4) \\ G^k(c_3 + ic_4) + \sqrt{3}M^k(ic_3 - c_4) & 0 & 0 & 0 \\ 0 & G^k(c_3 + ic_4) + \sqrt{3}M^k(-ic_3 + c_4) & 0 & 0 \end{bmatrix}. \tag{2}$$

Finally, we focus on the sixfold-degenerate point at the R position, and it is situated in the frequency range of 3.80–3.85 THz. Different from the electronic systems, this sixfold-degenerate point corresponds to the maximum degeneracy in such spinless phononic systems. Such SDP exhibits different band dispersion situations along the Γ-R-M path, i.e., four bands with two doubly degenerate bands in the Γ-R part and five bands with one doubly degenerate band in the R-M part. A complete band surface has been calculated in the $k_y = \pi$ plane, and the results are shown in Fig. 4(a), where the white dot corresponds to the SDP. Note that only a very small part of the surface band dispersions around the R position is shown here due to the complex band shapes and overlaps. Due to the six-dimensional irreducible representation at the R position, the effective Hamiltonian can be constructed by Eq. (3), where c_is are real parameters. The surface states of this SDP are further computed along the (001) plane projection and are reported in Fig. 4(d). The corresponding band dispersion along the same path is shown in Fig. 4(c) as a comparison. Since the SDP does not carry net Berry curvature, its surface states are not strictly protected by the band topology. However, two large arc surface states are observed in Fig. 4(d), as indicated by the white arrows, and they both come from the projected point of the white dot at the $\tilde{R}$ position. Different from the previous two points with quadratic order, this SDP shows a clear linear band dispersion, and the two arc states are only from the sixfold degeneracy instead of the quadratic order [32]. In contrast to the internal arc state, the external one can be completely distinguished from the bulk states, and thus it is advantageous for experimental observation:

$$H_{\mathrm{SP}}(\mathbf{k}) = \begin{bmatrix} 0 & 0 & -ic_1k_z & ic_1k_y & ic_2k_z & -ic_2k_y \\ 0 & 0 & -ic_2k_z & -ic_2k_y & ic_1k_z & ic_1k_y \\ ic_1k_z & ic_2k_z & 0 & ic_1k_x & 0 & ic_2k_x \\ -ic_1k_y & ic_2k_y & -ic_1k_x & 0 & -ic_2k_x & 0 \\ -ic_2k_z & -ic_1k_z & 0 & ic_2k_x & 0 & ic_1k_x \\ ic_2k_y & -ic_1k_y & -ic_2k_x & 0 & -ic_1k_x & 0 \end{bmatrix}. \tag{3}$$

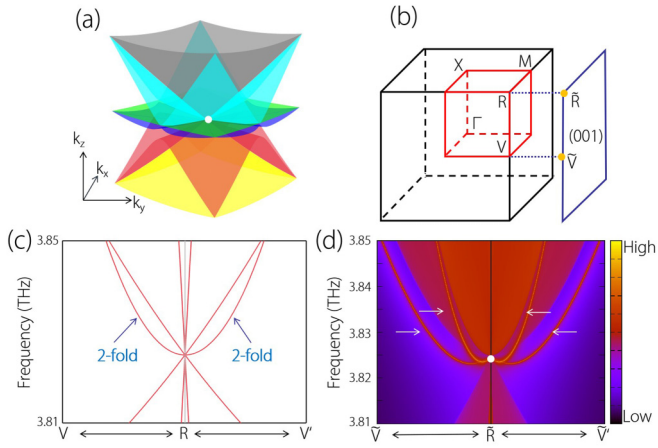

FIG. 4. The calculated phonon dispersion (a) around the SDP, which is highlighted by the white dot. The (001) surface projection (b) of the bulk Brillouin zone. The local enlargement of the phonon band dispersion around the QCDP (c) and the corresponding (001) surface-states projection, with the two arc-shaped spectra indicated by the white arrow.

IV. CONCLUSIONS

In this article, through a systematic theoretical investigation we proposed a realistic compound Ta_3Sn with $Pm\bar{3}n$ structure, and it hosts two quadratic orders and one sixfold-degenerate phononic nodal point. The QCTP is located at the Γ position, and the other QCDP and SDP are situated at the R position but with different frequency ranges. To show their formation mechanism, precise band-surface calculations have been performed and revealed individually, and effective Hamiltonian models have also been constructed for each nodal point. Additionally, the corresponding surface states are computed, and clear surface arc states originating from these projected nodal points are all observed. To our best knowledge, the phononic nodal point with quadratic order or sixfold degeneracy is much less studied in previous research, and their coexistence in a single material is even rarer. Considering the spinless feature and the negligible spin-orbital coupling effect in phononic systems, the current material can serve as an ideal platform to study the topological states related with nodal points of quadratic order and sixfold degeneracy. Further experimental investigations and verification for these phononic points are expected.

ACKNOWLEDGMENTS

This work is supported by the Natural Science Foundation of Chongqing (No. cstc2021jcyj-msxmX0376 and No. cstc2018jcyjA0765) and the National Natural Science Foundation of China (No. 51801163). The authors also want to acknowledge helpful discussions with Dr. Ying Liu.

[1] L. Fu, C. L. Kane, and E. J. Mele, Phys. Rev. Lett. **98**, 106803 (2007).
[2] X.-L. Qi and S.-C. Zhang, Rev. Mod. Phys. **83**, 1057 (2011).
[3] A. Bansil, H. Lin, and T. Das, Rev. Mod. Phys. **88**, 021004 (2016).
[4] B. Bradlyn, L. Elcoro, J. Cano, M. G. Vergniory, Z. Wang, C. Felser, M. I. Aroyo, and B. A. Bernevig, Nature (London) **547**, 298 (2017).
[5] B. Yan and C. Felser, Annu. Rev. Condens. Matter Phys. **8**, 337 (2017).
[6] H. Gao, J. W. Venderbos, Y. Kim, and A. M. Rappe, Annu. Rev. Mater. Res. **49**, 153 (2019).
[7] T. Zhang, Y. Jiang, Z. Song, H. Huang, Y. He, Z. Fang, H. Weng, and C. Fang, Nature (London) **566**, 475 (2019).
[8] A. A. Burkov, Nat. Mater. **15**, 1145 (2016).
[9] W. C. Yu, X. Zhou, F.-C. Chuang, S. A. Yang, H. Lin, and A. Bansil, Phys. Rev. Mater. **2**, 051201(R) (2018).
[10] Z.-M. Yu, W. Wu, Y. X. Zhao, and S. A. Yang, Phys. Rev. B **100**, 041118(R) (2019).
[11] S. A. Yang, H. Pan, and F. Zhang, Phys. Rev. Lett. **113**, 046401 (2014).
[12] W. Wu, Y. Liu, S. Li, C. Zhong, Z.-M. Yu, X.-L. Sheng, Y. X. Zhao, and S. A. Yang, Phys. Rev. B **97**, 115125 (2018).
[13] Y. Xia and G. Li, Phys. Rev. B **96**, 241204(R) (2017).
[14] C. Fang, Y. Chen, H.-Y. Kee, and L. Fu, Phys. Rev. B **92**, 081201(R) (2015).
[15] A. A. Burkov, M. D. Hook, and L. Balents, Phys. Rev. B **84**, 235126 (2011).
[16] X. Feng, C. Yue, Z. Song, Q. S. Wu, and B. Wen, Phys. Rev. Mater. **2**, 014202 (2018).
[17] D.-F. Shao, G. Gurung, S.-H. Zhang, and E. Y. Tsymbal, Phys. Rev. Lett. **122**, 077203 (2019).
[18] T.-R. Chang, I. Pletikosic, T. Kong, G. Bian, A. Huang, J. Denlinger, S. K. Kushwaha, B. Sinkovic, H.-T. Jeng, T. Valla, W. Xie, and R. J. Cava, Adv. Sci. **6**, 1800897 (2019).
[19] T. He, X. Zhang, Y. Liu, X. Dai, G. Liu, Z.-M. Yu, and Y. Yao, Phys. Rev. B **102**, 075133 (2020).
[20] P. B. Pal, Am. J. Phys. **79**, 485 (2011).
[21] X. Zhang, L. Jin, X. Dai, and G. Liu, J. Phys. Chem. Lett. **8**, 4814 (2017).
[22] X. M. Zhang, Z. M. Yu, Z. M. Zhu, W. K. Wu, S. S. Wang, X. L. Sheng, and S. A. Yang, Phys. Rev. B **97**, 235150 (2018).
[23] J. Liu and D. Vanderbilt, Phys. Rev. B **90**, 155316 (2014).
[24] C. Chen, Z.-M. Yu, S. Li, Z. Chen, X.-L. Sheng, and S. A. Yang, Phys. Rev. B **99**, 075131 (2019).
[25] T. Yang, Y. Liu, Z. Wu, X. Wang, and G. Zhang, Mater. Today Phys. **18**, 100348 (2021).
[26] Z. Zhu, G. W. Winkler, Q. S. Wu, J. Li, and A. A. Soluyanov, Phys. Rev. X **6**, 031003 (2016).
[27] C. K. Barman, C. Mondal, B. Pathak, and A. Alam, Phys. Rev. B **99**, 045144 (2019).
[28] Q. Ma, S.-Y. Xu, C.-K. Chan, C.-L. Zhang, G. Chang, Y. Lin, W. Xie, T. Palacios, H. Lin, S. Jia, P. A. Lee, P. Jarillo-Herrero, and N. Gedik, Nat. Phys. **13**, 842 (2017).
[29] T. Yang, G. Ding, Z. Cheng, X. Wang, and G. Zhang, J. Mater. Chem. C **8**, 7741 (2020).
[30] T. Yang, Z. Cheng, X. Wang, and X.-L. Wang, J. Adv. Res. **28**, 43 (2021).
[31] N. Kumar, M. Yao, J. Nayak, M. G. Vergniory, J. Bannies, Z. Wang, N. B. M. Schroeter, V. N. Strocov, L. Muechler, W. Shi, E. D. L. Rienks, J. L. Manes, C. Shekhar, S. S. P. Parkin, J. Fink, G. H. Fecher, Y. Sun, B. A. Bernevig, and C. Felser, Adv. Mater. **32**, 1906046 (2020).
[32] S. Nie, B. A. Bernevig, and Z. Wang, Phys. Rev. Res. **3**, L012028 (2021).
[33] R. Chapai, Y. Jia, W. A. Shelton, R. Nepal, M. Saghayezhian, J. F. DiTusa, E. W. Plummer, C. Jin, and R. Jin, Phys. Rev. B **99**, 161110(R) (2019).
[34] T. Yang, L. Jin, Y. Liu, X. Zhang, and X. Wang, Phys. Rev. B **103**, 235140 (2021).
[35] X. Yang, T. A. Cochran, R. Chapai, D. Tristant, J.-X. Yin, I. Belopolski, Z. Cheng, D. Multer, S. S. Zhang, N. Shumiya, M. Litskevich, Y. Jiang, G. Chang, Q. Zhang, I. Vekhter, W. A. Shelton, R. Jin, S.-Y. Xu, and M. Z. Hasan, Phys. Rev. B **101**, 201105(R) (2020).
[36] L. Jin, X. Zhang, Y. Liu, X. Dai, X. Shen, L. Wang, and G. Liu, Phys. Rev. B **102**, 125118 (2020).
[37] T. He, Y. Liu, L. Tian, X. Zhang, W. Meng, X. Dai, and G. Liu, Phys. Rev. B **103**, 085135 (2021).
[38] T. Yang and X. Zhang, J. Mater. Chem. C **8**, 9046 (2020).
[39] P. Wölfle, Rep. Prog. Phys. **81**, 032501 (2018).
[40] N. Laflorencie, Phys. Rep. **646**, 1 (2016).
[41] O. Stenull, C. L. Kane, and T. C. Lubensky, Phys. Rev. Lett. **117**, 068001 (2016).
[42] Z. J. Chen, R. Wang, B. W. Xia, B. B. Zheng, Y. J. Jin, Y.-J. Zhao, and H. Xu, Phys. Rev. Lett. **126**, 185301 (2021).
[43] C. Xie, Y. Liu, Z. Zhang, F. Zhou, T. Yang, M. Kuang, X. Wang, and G. Zhang, Phys. Rev. B **104**, 045148 (2021).
[44] Q.-B. Liu, Z. Wang, and H.-H. Fu, Phys. Rev. B **103**, L161303 (2021).
[45] T. Zhang, Z. Song, A. Alexandradinata, H. Weng, C. Fang, L. Lu, and Z. Fang, Phys. Rev. Lett. **120**, 016401 (2018).
[46] H. Miao, T. T. Zhang, L. Wang, D. Meyers, A. H. Said, Y. L. Wang, Y. G. Shi, H. M. Weng, Z. Fang, and M. P. M. Dean, Phys. Rev. Lett. **121**, 035302 (2018).
[47] M. Zhong, Y. Liu, F. Zhou, M. Kuang, T. Yang, X. Wang, and G. Zhang, Phys. Rev. B **104**, 085118 (2021).
[48] S. Singh, Q. S. Wu, C. Yue, A. H. Romero, and A. A. Soluyanov, Phys. Rev. Mater. **2**, 114204 (2018).
[49] W. Wu, Z.-M. Yu, X. Zhou, Y. X. Zhao, and S. A. Yang, Phys. Rev. B **101**, 205134 (2020).
[50] Z.-M. Yu, W. Wu, X.-L. Sheng, Y. X. Zhao, and S. A. Yang, Phys. Rev. B **99**, 121106(R) (2019).
[51] Z. Zhang, Z.-M. Yu, and S. A. Yang, Phys. Rev. B **103**, 115112 (2021).
[52] Z. Yu, Z. Zhang, G.-B. Liu, W. Wu, X.-P. Li, R.-W. Zhang, S. Yang, and Y. Yao, Sci. Bull. **67**, 375 (2022).
[53] T. Zhang, R. Takahashi, C. Fang, and S. Murakami, Phys. Rev. B **102**, 125148 (2020).
[54] M. C. Payne, M. P. Teter, D. C. Allan, T. A. Arias, and J. D. Joannopoulos, Rev. Mod. Phys. **64**, 1045 (1992).
[55] J. Hafner, J. Comput. Chem. **29**, 2044 (2008).

[56] P. E. Blöchl, Phys. Rev. B **50**, 17953 (1994).
[57] M. Ernzerhof and G. E. Scuseria, J. Chem. Phys. **110**, 5029 (1999).
[58] J. P. Perdew, K. Burke, and M. Ernzerhof, Phys. Rev. Lett. **77**, 3865 (1996).
[59] S. Geller, B. T. Matthias, and R. Goldstein, J. Am. Chem. Soc. **77**, 1502 (1955).
[60] A. Togo and I. Tanaka, Scr. Mater. **108**, 1 (2015).
[61] Q. Wu, S. Zhang, H.-F. Song, M. Troyer, and A. A. Soluyanov, Comput. Phys. Commun. **224**, 405 (2018).